Communications in Physics, Vol. 31, No. 1 (2021), pp. 57-65
DOI:10.15625/0868-3166/15319

IN SILICO PROBING Ca^{2+} AND Zn^{2+} PERMEABLE TRANSMEMBRANE $4A\beta_{1-42}$ BARREL

SON TUNG NGO[1,2,†]

[1]*Laboratory of Theoretical and Computational Biophysics, Ton Duc Thang University, Ho Chi Minh City, Vietnam*

[2]*Faculty of Applied Sciences, Ton Duc Thang University, Ho Chi Minh City, Vietnam*

E-mail: [†]ngosontung@tdtu.edu.vn

Received 28 July 2020
Accepted for publication 29 October 2020
Published 5 January 2021

Abstract. *Alzheimer's disease (AD) is known as one of the most popular forms of dementia affecting numerous people worldwide. The Amyloid beta (Aβ) peptides form oligomeric conformations that cause the intracellular Ca^{2+} and Zn^{2+} abnormality leading to the death of neuron cells. The failure of AD therapy targeting Aβ oligomers probably caused by misunderstanding the ions transport through transmembrane Aβ (tmAβ) ion-like channel since Aβ oligomers transiently exist in a mixture environment involving various order of Aβ oligomers. The high-resolution of tmAβ peptides are thus unavailable until the date. Fortunately, computational approaches are able to complement the missing experimental structures. The transmembrane $4A\beta_{1-42}$ ($tm4A\beta_{1-42}$) barrel, one of the most neurotoxic elements, was thus predicted in the previous work. Therefore, in this context, the Ca^{2+}/Zn^{2+} ions transport through the $tm4A\beta_{1-42}$ barrel was investigated by using the fast pulling of ligand (FPL) and umbrella sampling (US) methods. Good consistent results were obtained implying that Ca^{2+} ion transport through $tm4A\beta_{1-42}$ barrel with a lower free energy barrier compared with Zn^{2+} ion. The obtained results about Ca^{2+}/Zn^{2+} transport across $tmA\beta_{1-42}$ barrel probably enhances the AD therapy since we can design an inhibitor is able to block the transport.*

Keywords: Amyloid, Barrel, Ion-Like channel, Ca^{2+}, Zn^{2+}, US.

Classification numbers: 87.14.ep; 82.60.-s; 05.70.Ce; 51.30.+i; 65.40.G.

I. INTRODUCTION

Amyloid beta (Aβ) peptide is characterized as a critical element associating with Alzheimer's disease (AD), a neurodegenerative issue affecting several millions of elders [1, 2]. The Amyloid

cascade hypothesis was proffered to explain the nature of AD and it is widely accepted with many preclinical and clinical investigations [3]. Initially, the supporter of the Amyloid cascade hypothesis believed that Aβ fibrils are a critical factor poisoning the patient brain, but the Aβ oligomers are then indicated as the neurotoxicity forms since generating the ion channel-like structure allowing ion Ca^{2+} crossing [2]. The oligomers are intermediate of self-aggregating Aβ peptides from disorder states to mature fibrils. The structures of Aβ oligomers have not been explored in experiments since they stay in the mixture environment including several various order oligomers and fibrils [4, 5]. On another hand, the Aβ peptide is a rapid self-aggregating peptide, the intermediate shapes of the self-aggregating progress including oligomeric configurations are hard to be detected.

Most scientists believe that the β-content is equated with neurotoxicity since the population of the conformation is detected in Aβ aggregated forms. Therefore, rich β-content oligomers are often considered to be a highly toxic agent. Several investigations of Aβ oligomeric shapes have been carried out with the criteria to determine these conformations are related to β-content of Aβ peptides [6]. The potential inhibitors for Aβ peptides are thus searched focusing on demolishing the Aβ conformations having high β-content [7]. Both *in silico* and *in vitro* the aggregated structures of Aβ peptides are inhibited, but the drug candidates targeting Aβ peptides are almost failed in clinical trials [8–10]. Therefore, unfortunately, after 27^{th} years of this hypothesis, the searching for a potential drug is a failure currently [11, 12].

The formation of a transmembrane ion channel-like structure of Aβ peptides leads to the death of neuron cells since it disturbs the ion Ca^{2+} concentration. The existence of these structures has been observed using Atomic Force Microscopy [13, 14]. Although, the experimental high resolution of these structures is still lacked, the transmembrane structures of Aβ peptides are recently proposed using rigorous simulations fortunately [15, 16]. It is very important since it is able to explain how Aβ oligomer disturbs the ion Ca^{2+} homeostasis [17]. Ca^{2+} crossing the helical transmembrane $A\beta_{1-42}$ tetramer (*tm*$4A\beta_{1-42}$) was thus investigated using a incorporation of replica exchange molecular dynamics (REMD) and umbrella sampling (US) simulations [15]. However, the ion-permeable the *tm*$4A\beta_{1-42}$ barrel is still unknown. Moreover, although Zn^{2+} ion was much less considered than Ca^{2+} ion, intracellular Zn^{2+} abnormality is recently reported that it is associated with neurodegeneration and cognitive decline than intracellular Ca^{2+} abnormality [18]. Zn^{2+} ion was also bound to Aβ ion-like channel with a high affinity, resulting in blocking and modulating the Aβ channel [19]. Preventing intracellular Ca^{2+} and Zn^{2+} abnormality is raised as one of the promising AD therapy [20]. Therefore, in this context, the Ca^{2+} and Zn^{2+}permeable the *tm*$4A\beta_{1-42}$ barrel is thus investigated using steered molecular dynamics (SMD) simulations. The obtained results are probably added to existing knowledge and may help to enhance AD treatment.

II. MATERIALS AND METHODS

II.1. Starting structure of the Ca^{2+}/Zn^{2+} + *tm*$4A\beta_{1-42}$

The *tm*$4A\beta_{1-42}$ peptide was obtained from the previous work [16], which was generated over 500 ns of REMD simulations. In this work, the peptide was still parameterized via the united-atom GROMOS 53a6 force field [21]. The peptide was fully inserted into the DPPC lipid bilayers [22]. The ions were topologized via the GROMOS 53a6 force field. In particular, the

water molecules were substituted by Ca^{2+}/Zn^{2+} ions at the selected position as shown in Fig. 1 (the blue ball). The additional ion Cl^{-} atoms were added to neutralize the soluble systems. Therefore, the Ca^{2+}/Zn^{2+} + *tm*4Aβ_{1-42} system consists of 1 Ca^{2+}/Zn^{2+}, 4 Aβ peptides, 123 DPPC molecules, 4912 water molecules, 2 Cl^{-} ions, and neutralized 12 Na^{+} ions (total atoms of 22537). The system was placed into a rectangular periodic boundary condition box, denoted as PBC, with a size of $63.8 \times 64.0 \times 77.4$ Angstrom. The initial structure of the Ca^{2+}/Zn^{2+} + *tm*4Aβ_{1-42} systems were shown in Fig. 1.

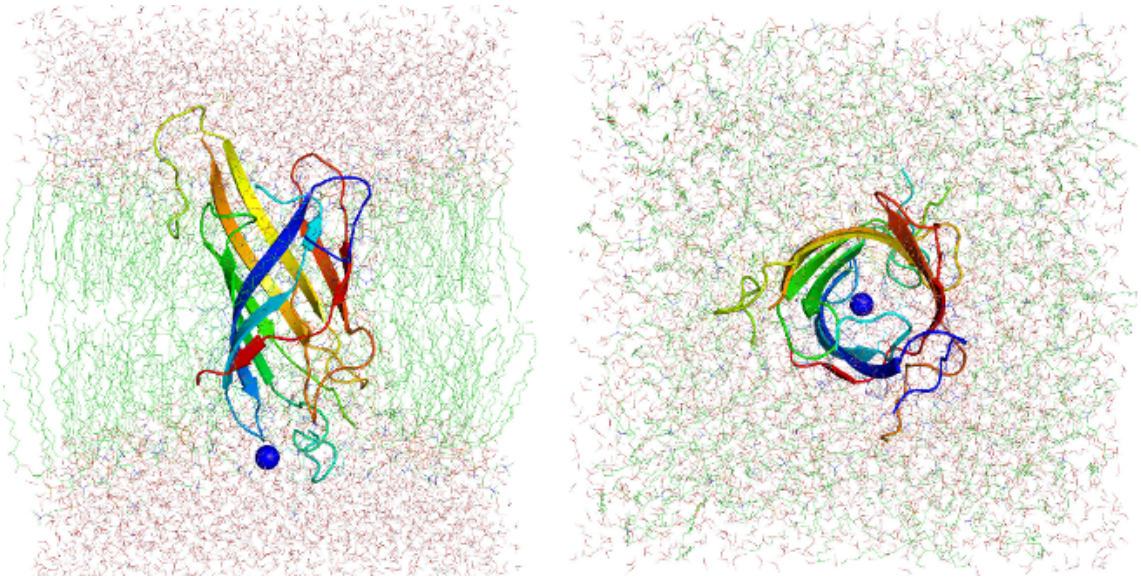

Fig. 1. The starting conformation of the Ca^{2+}/Zn^{2+} + tm*4A*β_{1-42} system in different view-orientations. Blue ball represents the Ca^{2+}/Zn^{2+} ion.

II.2. Molecular dynamics (MD) simulation

GROMACS version 5.1.5 [23] was operated to replicate the Ca^{2+}/Zn^{2+} + *tm*4Aβ_{1-42} system. The MD simulations were executed with the specifications denoted to the earlier probes [24]. Particularly, the MD time step is 2 fs. The nonbonded pair was influenced within a radius of 9 Angstrom. The Coulomb interaction was enumerated via the fast Particle-Mesh Ewald electrostatics interpretation [25]. The Ca^{2+}/Zn^{2+} + *tm*4Aβ_{1-42} system was then minimized and equilibrated over energic minimization (EM), canonical (NVT), and isothermal-isobaric (NPT) simulations. The length of NVT and NPT simulations was length of 0.1 ns. During NVT simulation, the *tm*4A$\beta_{1-42}C_{\alpha}$ atoms and Ca^{2+}/Zn^{2+} ions were impelled by implementing an inadequate harmonic force with a amount of 1000 kJ $mol^{-1}nm^{-2}$ per dimensions. The equilibrated shape of the Ca^{2+}/Zn^{2+} + *tm*4Aβ_{1-42} system was subsequently employed as the initial shape of SMD simulations with a total interval of 0.8 ns.

II.3. FPL simulation

The final conformation of isobaric-isothermal imitations was engaged as the starting shape for FPL simulation [26]. Computational investigations were espoused to the prior examinations [26]. In specific, the initial structure of SMD simulations is shown in Fig. 2. The spring constant cantilever, k, and pulling velocity, v, were chosen as 600 kJ mol^{-1} nm^{-2} and 0.005 nm ps^{-1}, correspondingly. During the atomistic computations, the C_α atoms of *tm*Aβ_{1-42} peptide were positionally impeded using an inadequate harmonic potential. An external harmonic force was put on the Ca^{2+}/Zn^{2+} ions to force the ion to mobilize across the ion-like channel. (cf. Fig. 2). The ionic transposition and value of pulling force forwards Z-orientation were tracked each interval of 0.1 ps. The FPL assessments were reduplicated with 100 independent times to assurance the sampling of assessments.

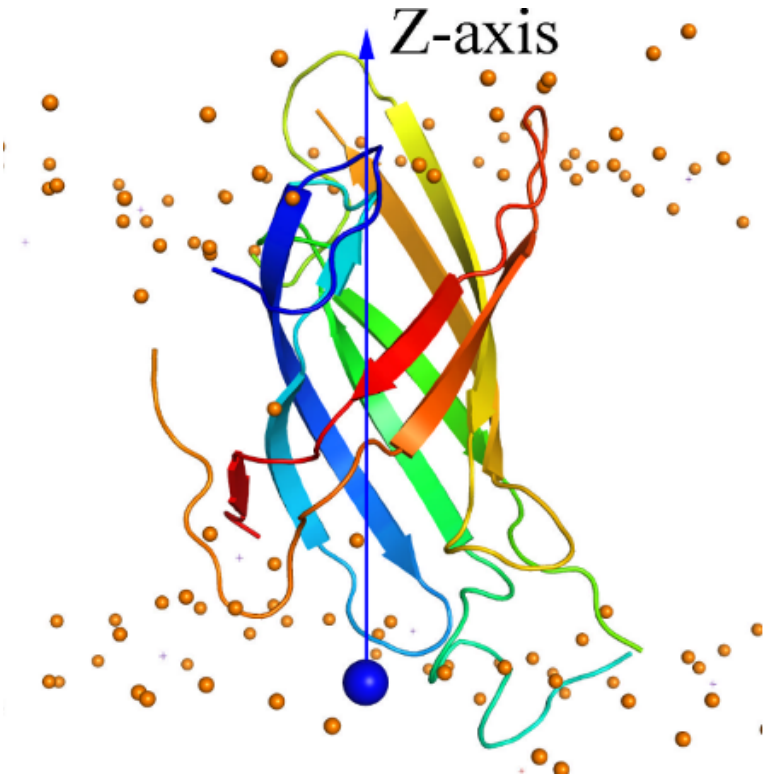

Fig. 2. The initial conformation of SMD simulations. The Ca^{2+}/Zn^{2+} ions were forced to mobilize across the *tm*4Aβ_{1-42} peptide along Z-axis.

II.4. US simulation

The free energy terms of Ca^{2+}/Zn^{2+} ions along Z-orientation, reaction coordinate ξ, was appraised via the US scheme [27]. The FPL mimicking was manipulated to produce the investigated shapes of the US simulations. The Ca^{2+}/Zn^{2+} atoms were mobilized along Z-axis as mentioned above. Several shapes along the ξ was created with the spacing of ca. 3 Å as referring

to the previous study [15]. These shapes were manipulated as the commencing inputs of the US assessments with a length of 30 ns per windows, in which the first 10 ns in each window was disbanded from the analysis to avoid any initial bias. The difference of free energy, ΔG, of ion Ca^{2+}/Zn^{2+} passing the barrier was assessed from the potential of mean force, noted as PMF, via the weighted histogram analysis, noted as WHAM, protocol [28] with 100 rounds of bootstrapping calculation [29].

III. RESULTS AND DISCUSSION

We first reported an exhaustive analysis of the computations with GROMOS96 56a3/SPC force field about the conduction of Ca^{2+}/Zn^{2+} ions crossing *tm*4Aβ_{1-42} peptide via SMD and US simulations. The starting conformation of the *tm*4Aβ_{1-42} peptide was obtained from 500 ns of REMD simulations in the previous work [16] as shown in Fig. 1. It should be noted that the metastable structure was selected as conformation A of Ref. [16] and the structure occupied 48% of total snapshots of REMD simulations and its inner diameter pore was measured as 0.75 nm [16]. The structure of *tm*4Aβ_{1-42} peptide consists of 8-stranded β-sheets in antiparallel states that they construct 4 β-hairpins. The C_α atoms of the *tm*Aβ_{1-42} peptide were positionally restrained during the simulations to prevent any effects of external pulling force on the β-barrel structure.

III.1. Durability of DPPC lipid during simulation

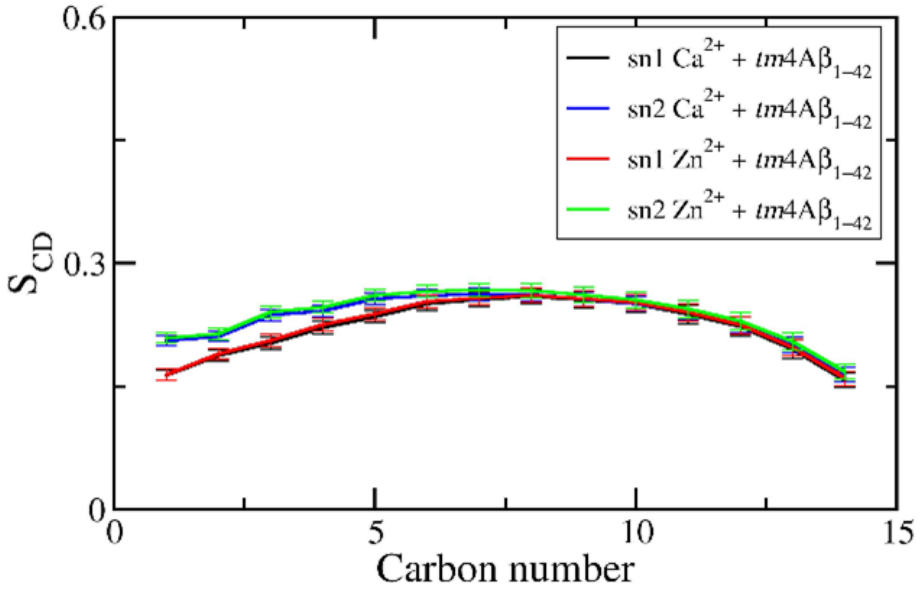

Fig. 3. (Color online) Lipid order parameters of carbon atoms of both acyl chains sn1 and sn2. The computed error is the standard deviation over 100 independent trajectories.

The influence of *tm*4Aβ_{1-42} peptide on the structure of DPPC lipid bilayers can be predicted through the investigation of lipid stabilization. Moreover, investigating lipid durability also revealed that applying external force does not disrupt the system. The stabilization of DPPC lipid bilayers during the MD simulations was thus estimated via the analysis of lipid order parameters.

The parameters were calculated for carbon atoms of both acyl chains **sn1** and **sn2** as shown in Fig. 3. The error of lipid order parameters $S_{CD} = \frac{1}{2}\overline{3cos^2\varphi - 1}$, where φ is the angle between the bilayer normal and $C_{i-1} - C_{i+1}$ vector, showing in Fig. 3 is the standard deviation that is estimated over 100 independent trajectories. The obtained values are in good consistency with the previous works [30–34], although the attained values differ from the isolated DPPC system [32]. The difference suggests the change of DPPC lipid bilayers under the effects of *tm*4Aβ_{1-42} peptide.

III.2. SMD simulation

As mentioned above, Aβ peptides are able to form ion-like channel structures that disturb the Ca^{2+} homeostasis since leaving the ion transport through these conformations. Clarifying the physical insights into the ion transference over the *tm*Aβ peptides is thus of great interest. However, studying the issue using the unrestrained MD simulations will be required a huge CPU time consumption. Therefore, the FPL scheme [26] was utilized to estimate the free energy barrier of Ca^{2+}/Zn^{2+} ion crossing *tm*4Aβ_{1-42} system that results were shown in Table 1 and Fig. 4. Moreover, it should be noted that we may argue that the ion transport through *tm*Aβ peptides with a larger free energy barrier probably requires a larger pulling force to oblige the ion across the Aβ ion-like channels. The reason is probably explained that the ion required a larger free energy barrier possibly has a larger binding affinity to the Aβ peptide. Table 1 demonstrated that the Zn^{2+} ion required a larger pulling force to mobilize across the *tm*4Aβ_{1-42} barrel in comparison with the Ca^{2+} ion. The obtained results implied that Zn^{2+} has a large binding affinity to *tm*Aβ peptide, resulting in blocking the transport of Ca^{2+} crossing Aβ channel [35].

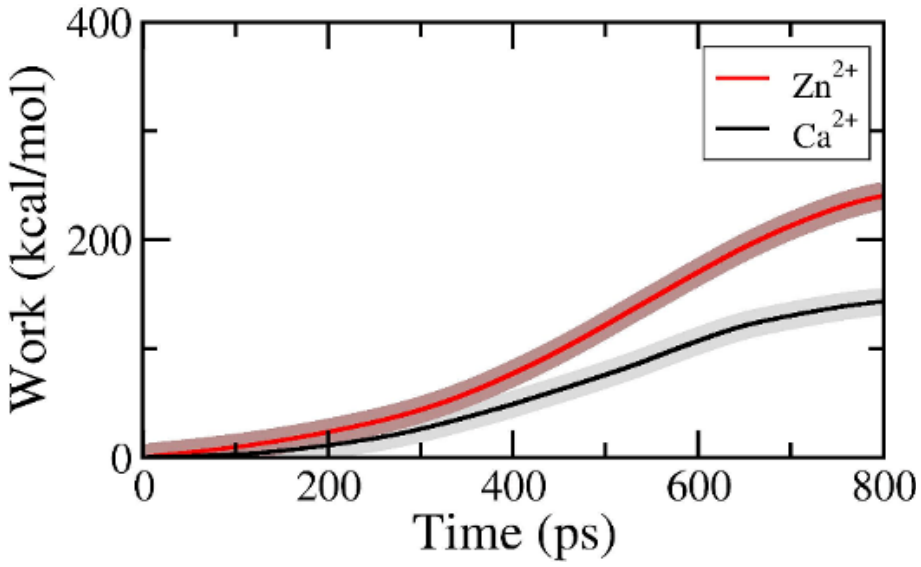

Fig. 4. (Color online) The mean pulling work $< \boldsymbol{W} >$ of external force over 100 independent SMD trajectories, which was calculated via formula $\boldsymbol{W} = \boldsymbol{v}\int_0^t \boldsymbol{F}(t)\,\boldsymbol{dt}$, where $\boldsymbol{v}$ is pulling speed and $\boldsymbol{F}$ is pulling force. The blurred area along $< \boldsymbol{W} >$ mentioned the assessed error, which was calculated as the standard error of the average.

Table 1. The obtained results from SMD and US simulations.

	$< F_{max} >$ (pN)[a]	$< W >$ (kcal mol^{-1})[b]	ΔG (kcal mol^{-1})[c]
Zn^{2+}	1206.1 ± 15.6	240.5 ± 3.8	26.6 ± 3.2
Ca^{2+}	822.5 ± 13.8	144.5 ± 3.4	18.9 ± 1.2

The average values of pulling force[a] and work[b] over 100 independent SMD trajectories.
The free energy barrier ΔG obtained via US simulations.

III.3. US simulation

The US simulation was employed to confirm the obtained results of FPL calculations above. The FPL trajectory was used to generate initial conformations of US simulations. In particular, the Ca^{2+}/Zn^{2+} ion coordinate was recorded every 0.3 nm to use as initial structures of biased sampling calculation. Each US window was produced via 30 ns of MD simulations. Therefore, the free energy values ahead the ξ were computed over the US windows via a GROMACS tool named "wham" [28]. The achieved outcome were represented in Fig. 5. Although the attitude of free energy curves are roughly similar together, the Zn^{2+} ion weakly bound to Aβ at the beginning of the simulations. Then, the Zn^{2+} free energy metrics quickly raised when the ion mobilized around the end of the channel. Therefore, the free energy barrier of Zn^2 is significantly larger than that of Ca^{2+} ion (cf. Table 1 and Fig. 5). It may happen since Zn^{2+} ion probably forms a larger interaction with Glu9, His13, and His14 residues than Ca^{2+}ion does. Moreover, the ΔG of Ca^{2+} crossing $tm4A\beta_{1-42}$ is slightly larger than that of Ca^{2+} across S6 pore of the voltage-gated calcium channel RyR1 (PDB ID 5TAL [36]), which was computed of 16.88 ± 1.24 kcal/mol. Overall, the consistent observation between FPL and US simulations confirmed that Ca^{2+} ion is easier to mobilize through $tm4A\beta_{1-42}$ peptide than Zn^{2+} ion does.

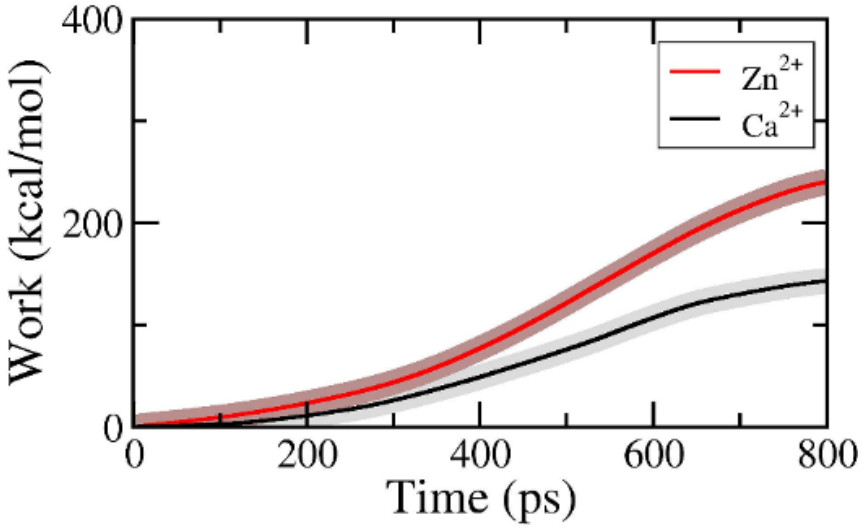

Fig. 5. (Color online) Free energy profile of Ca^{2+}/Zn^{2+} crossing $tm4A\beta_{1-42}$ system.

IV. CONCLUSIONS

The transport of Ca^{2+} and Zn^{2+} ions through *tm*4Aβ_{1-42} peptide was studied by using both the FPL and US simulations. Good consistent results were obtained implying that Ca^{2+} ion transport through *tm*4Aβ_{1-42} barrel with a lower free energy barrier compared with Zn^{2+} ion. It probably occurs since Zn^{2+} ion probably has a strong interaction with Glu9, His13, and His14 residues than Ca^{2+}ion does. Moreover, according to the US results, Ca^{2+} ion was indicated that the ion favorably interacts with Aβ C-terminal than the N-terminal, while Zn^{2+} ion adopts stronger binding to the N-terminal of *tm*Aβ_{1-42} barrel than the C-terminal one. Furthermore, the free energy barrier Ca^{2+} across the *tm*4Aβ_{1-42} is approximately the same range with crossing calcium channel S6. *Overall*, obtained results about Ca^{2+}/Zn^{2+} transport across *tm*Aβ_{1-42} barrel may help to enhances the AD therapy.

ACKNOWLEDGEMENTS

This work is funded by Vietnam National Foundation for Science & Technology Development (NAFOSTED) under the grant number 104.99-2019.57.

REFERENCES

[1] D. J. Selkoe, *Neuron* **6** (1991) 487.
[2] H. W. Querfurth, F. M. LaFerla, *N. Engl. J. Med.* **362** (2010) 329.
[3] D. J. Selkoe, J. Hardy, *EMBO Mol. Med.* **8** (2016) 595.
[4] G. Bitan, M. D. Kirkitadze, A. Lomakin, S. S. Vollers, G. B. Benedek and D. B. Teplow, *Proc. Natl. Acad. Sci. U.S.A.* **100** (2003) 330.
[5] M. D. Kirkitadze, M. M. Condron and D. B. Teplow, *J. Mol. Biol.* **312** (2001) 1103.
[6] S. T. Ngo, H. M. Hung, D. T. Truong, M. T. Nguyen, *Phys. Chem. Chem. Phys.* **19** (2017) 1909.
[7] S. T. Ngo, D. T. Truong, N. M. Tam and M. T. Nguyen, *J. Mol. Graph. Model.* **76** (2017) 1-10.
[8] L. M. Jarvis, *Chem. Eng. News* **90** (2012) 8.
[9] A. Abbott and E. Dolgin, *Nature* **540** (2016) 15.
[10] F. Panza, V. Solfrizzi, B.P. Imbimbo, G. Logroscino, *Expert Opin. Biol. Ther.* **14** (2014) 1465.
[11] W. I. Rosenblum, *Neurobiol Aging* **35** (2014) 969.
[12] A. J. Doig, M. P. del Castillo-Frias, O. Berthoumieu, B. Tarus, J. Nasica-Labouze, F. Sterpone, P. H. Nguyen, N. M. Hooper, P. Faller and P. Derreumaux, *ACS Chem Neurosci* **8** (2017) 1435.
[13] R. Lal, H. Lin, A.P. Quist, *BBA - Biomembranes* **1768** (2007) 1966.
[14] L. Connelly, H. Jang, F. T. Arce, R. Capone, S. A. Kotler, S. Ramachandran, B. L. Kagan, R. Nussinov and R. Lal, *J. Phys. Chem. B* **116** (2012) 1728.
[15] S.T. Ngo, P. Derreumaux, V.V. Vu, *J. Phys. Chem. B* **123** (2019) 2645.
[16] P.H. Nguyen, J.M. Campanera, S.T. Ngo, A. Loquet, P. Derreumaux, *J. Phys. Chem. B* **123** (2019) 3643.
[17] L. Tran, N. Basdevant, C. Prévost, T. Ha-Duong, *Scientific Reports* **6** (2016) 21429.
[18] H. Tamano, A. Takeda, *Biol. Pharm. Bull.* **42** (2019) 1070.
[19] N. Arispe, H.B. Pollard, E. Rojas, *Proc. Natl. Acad. Sci. U.S.A* **93** (1996) 1710.
[20] C. Corona, A. Pensalfini, V. Frazzini, S. L. Sensi, *Cell Death Dis.* **2** (2011) e176-e.
[21] C. Oostenbrink, A. Villa, A. E. Mark, W. F. Van Gunsteren, *J. Comput. Chem.* **25** (2004) 1656-76.
[22] J.F. Nagle, *Biophys. J.* **64** (1993) 1476.
[23] M. J. Abraham, T. Murtolad, R. Schulz, S. Pálla, J. C. Smith, B. Hessa and E. Lindahl, *SoftwareX* **1–2** (2015) 19.
[24] S. T. Ngo, *Comm. Phys.* **28** (2018) 265.
[25] T. Darden, D. York, L. Pedersen, *J. Chem. Phys.* **98** (1993) 10089.
[26] S. T. Ngo, H. M. Hung, M. T. Nguyen, *J. Comput. Chem.* **37** (2016) 2734.
[27] G. M. Torrie, J. P. Valleau, *J. Comput. Phys.* **23** (1977) 187.
[28] J. S. Hub, B.L. de Groot, D. van der Spoel, *J. Chem. Theory Comput.* **6** (2010) 3713.

[29] B. Efron. *Ann. Stat.* **7** (1979) 1.
[30] H. I. Petrache, S.W. Dodd, M. F. Brown, *Biophys. J.* **79** (2000) 3172.
[31] S. T. Ngo, M. T. Nguyen, N. T. Nguyen, V. V. Vu, *J. Phys. Chem. B* **121** (2017) 8467.
[32] S. T. Ngo, H. M. Hung, K. N. Tran, M. T. Nguyen, *RSC Adv.* **7** (2017) 7346.
[33] D. P. Tieleman, S.J. Marrink, H.J.C. Berendsen, *BBA-Rev. Biomembranes* **1331** (1997) 235.
[34] H. M. Hung, V. P. Nguyen, S. T. Ngo, M. T. Nguyen, *BioPhys. Chem.* **217** (2016) 1.
[35] C. Di Scala, N. Yahi, S. Boutemeur, A. Flores, L. Rodriguez, H. Chahinian, et al., *Sci. Rep*. **6** (2016) 28781.
[36] A. des Georges, O. B. Clarke, R. Zalk, Q. Yuan, K. J. Condon, R. A. Grassucci, W. A. Hendrickson, A. R Marks and J. Frank, *Cell* **167** (2016) 145-57.e17.